GEOPHYSICAL RESEARCH LETTERS, VOL. 36, L20502, doi:10.1029/2009GL039798, 2009

Surface melt area variability of the Greenland ice sheet: 1979–2008

Indrajit Bhattacharya,[1] Kenneth C. Jezek,[1] Lei Wang,[2] and Hongxing Liu[3,4]

Received 26 June 2009; revised 17 August 2009; accepted 22 September 2009; published 31 October 2009.

[1] The surface melt-area time-series (1979–2008) of the Greenland Ice Sheet (GrIS) shows large spatio-temporal variability. The overall melt-area time-series is characterized by a step-like increase in 1995. The melt-area trend for the entire ice-sheet between 1979–1994 is $7.64 \times 10^3 \pm 4.79 \times 10^3$km^2/year, which is 8-times higher than the period between 1995–2008 ($9.64 \times 10^2 \pm 1.10 \times 10^4$km^2/year). This step-like increase of melt area in 1995 coincides well with mean summer air temperature patterns at 8 coastal sites. We find that the melt area and temperature change in 1995, both coincide to a general sign-reversal in the North Atlantic Oscillation (NAO) index in 1995. We also find that the northerly sectors of the ice sheet do not clearly coincide with changes in the NAO suggesting the influence of NAO is being felt predominantly on the central-eastern and central-western sectors of the ice sheet. **Citation:** Bhattacharya, I., K. C. Jezek, L. Wang, and H. Liu (2009), Surface melt area variability of the Greenland ice sheet: 1979–2008, *Geophys. Res. Lett.*, *36*, L20502, doi:10.1029/2009GL039798.

1. Introduction

[2] Surface melting on the GrIS is an important indicator of Arctic terrestrial climate change much as the observations of dwindling Arctic sea-ice document climate change over the polar ocean [*Stroeve et al.*, 2008]. Space-borne passive microwave (PM) measurements show that the melt-area of the GrIS has increased since the start of observations in the 1970's to the present. Although reported estimates of absolute melt-area vary depending on parameters such as selected land-mask, algorithm and data sets, most investigators conclude that melt area is increasing at a linear rate somewhere between 0.6 to 1.8×10^4 km^2/year [*Abdalati and Steffen*, 1997; *Joshi et al.*, 2001; *Tedesco*, 2007; *Mote*, 2007] based on PM measurements.

[3] In this paper we adapt a recently developed PM algorithm [*Liu et al.*, 2005] to investigate both the spatial and temporal melt patterns across the GrIS. The Liu algorithm was successfully applied to measure surface melt across the Antarctic Ice Sheet [*Liu et al.*, 2006]. Their statistical method provides a more objective and precise melt onset-date, melt end-date and melt duration. After validating our estimates by comparison with an independent threshold based melt estimation technique [*Ashcraft and Long*, 2006] applied to the shorter time-series Quick Scatterometer (QuikSCAT), we show that the GrIS melt record includes important spatial and temporal patterns. In particular, we observe a persistent step-like increase in total melt area since 1995. The event appears to coincide with coastal summer temperature change and a general sign-reversal of the NAO index in 1995.

2. Data

[4] Primarily, we use three data sets: Brightness temperature (Tb) from Scanning Multichannel Microwave Radiometer (SMMR, 1979–1987), daily Tb data from Special Sensor Microwave Imager (SSM/I, 1987–2008) and daily backscatter (σ^0) data from QuikSCAT (2000–2008). For SMMR we used averaged, every alternate-day, polar-stereographic, Tb data gridded at 25km. The National Snow and Ice Data Center (NSIDC) SMMR polar stereographic product was selected because unlike the SMMR EASE grid product, it provides complete spatial coverage over the GrIS. However, a pixel in polar stereographic projection has an areal distortion of 4% at 81°N and −6% at 61°N latitude respectively, but these distortions are small in the context of our analysis. For SSM/I we use the EASE grid equal area projection data gridded at 25km. We chose ascending orbit data from F-11 and F-13 satellites for the period 1992–2008 and descending orbit data from F-8 satellite for the period 1989–1991 as these periods corresponds to the time of maximum daily melt. For a large number of days in 1994, ascending swath data over Greenland are missing, hence we substitute descending orbit data for 1994. Following *Liu et al.* [2006], we used 18GHz for SMMR and 19GHz for SSM/I (H-polarization for both) for our melt calculation.

[5] For QuikSCAT, we used 13GHz, V-polarized, polar stereographic data gridded at 4.45km. We use descending swath Version 1 Enhanced Resolution (QuikSCAT L1B) 'egg' data (rather than 'slice' data which has a higher noise level) for the period 2000–06. For Version 2 products from 2006–08, we use 'evening' σ^0 data for our melt calculation. The Greenland land mask for QuikSCAT was provided by D. Long at Brigham Young University.

[6] The Greenland land masks for EASE and polar stereographic grids are provided by NSIDC. We refined these three masks based on the snow classification map of Greenland (courtesy of National Survey and Cadastre, Denmark) and the RADARSAT-1 SAR mosaic of Greenland (courtesy of Ian Joughin). We also used NAO data (courtesy of NOAA) and air temperature records from 12 coastal weather stations that were available courtesy of NOAA, NASA, Royal Netherlands Meteorological Institute and Norwegian Meteorological Institute.

3. Method

3.1. Melt Detection From PM

[7] Melt is detectable in the PM time-series because of sharp changes in Tb associated with the presence of small

[1]Byrd Polar Research Center, Ohio State University, Columbus, Ohio, USA.
[2]Department of Geography and Anthropology, Louisiana State University, Baton Rouge, Louisiana, USA.
[3]Department of Geography, Texas A&M University, College Station, Texas, USA.
[4]Now at Department of Geography, University of Cincinnati, Cincinnati, Ohio, USA.

0094-8276/09/2009GL039798$05.00

amounts of water in the snowpack [*England*, 1976]. *Joshi et al.* [2001] applied an edge detection algorithm to the Tb time-series for surface melt detection over GrIS which was improved by *Liu et al.* [2005] by using a multi-scale wavelet transform technique. Melt detection is based on the observation that strong edges correspond to snow melting and refreezing events. Liu's statistical method used globally computed parameters, which proved acceptable for Antarctica where melting is generally limited to near coastal regions. Because there are stronger melt facies gradients across the smaller GrIS, we adapted the Liu method to include locally computed parameters.

[8] We divide GrIS into 10 sectors roughly corresponding to glacier drainages and based on surface slope and ice flow pattern (B. Csatho, personal communication, 2007) and further subdivide each sector into wet, percolation and dry snow facies (Figure 1a). The snow facies were delineated based on the relative change of σ^0 in the SAR mosaic; the wet facies can be observed very clearly towards the margin of the ice-sheet based on the presence of melt lakes; very low backscatter corresponds to darkest shades which correspond to dry snow facies in the central part of the ice-sheet and the region in-between the wet and the dry snow is the percolation facies. Because C-band radar penetrates several meters into the firn (which is equivalent of several years), the delineated facies boundary from the SAR image is ambiguous because of temporal smearing. Hence our dry snow facies boundary is conservative.

[9] Following the sector-wise division of the PM coverage of the ice-sheet, the annual Tb time-series of each pixel is decomposed using a multi-scale wavelet transform. We divide the annual Tb time-series into 'summer' and 'winter' and calculate a 'critical value' for the edge strengths during summer and winter periods for each year and for each pixel covering the ice-sheet. The critical value of a pixel is the edge strength which partitions the edges into two groups representing melt and non-melt events [*Liu et al.*, 2005]. Then for each pixel we compute the 10-year average of the critical values between 1995–2005 separately for summer and winter. Subsequently, we generate histograms of averaged summer-winter critical values for all pixels within each facies of each sector. We select a local 'optimal-threshold' for edges to identify melt events from these histograms. This local optimal threshold incorporates both the temporal and spatial variability of the edges strengths corresponding to melt events of a facies.

[10] To identify spurious edges caused by abrupt but subfreezing changes in physical temperature during the early spring, we apply an extra criterion. We check if the Tb for a pixel during any day is greater than half of the mean maximum Tb during the summer months. This Tb value is referred to as the 'outlier-threshold'. If the edge strength and the Tb value exceed both optimal-threshold and outlier-threshold, we consider the detected edge to be a valid melt event. Our algorithm depends on the relative change of Tb so we did not, in general inter-calibrate SMMR and SSM/I data. Because the operational lifespan of SMMR ended in mid August 1987 shortly after the start of SSM/I, we did calibrate the 1987 SSM/I data using the calibration coefficient from *Jezek et al.* [1993] so as to create a continuous time-series for 1987.

3.2. Melt Detection From QuikSCAT

[11] *Nghiem et al.* [2001], *Steffen et al.* [2004] and *Wang et al.* [2007] used QuikSCAT data to estimate surface melt and melt intensity from decrease in σ^0 associated with melt onset. Based on a snow backscatter model, *Ashcraft and Long* [2006] suggested that a wet snow layer of 3.8 cm thickness and 1% of liquid moisture content results in a -2.7 dB decrease in σ^0. Careful observation of σ^0 time-series for melt pixels shows that the decrease in σ^0 due to the presence of water can be gradual and only reaches a minimum after more than 2–3 days. So, our melt start criterion is: if within 3 consecutive days σ^0 decreases by 3 dB, then we designate this decrease as a signal for melt onset. Detection of end-of-melt is tricky because refreeze can result in a sudden increase in σ^0 by over 10 dB. *Zabel et al.* [1995] reported that development of ice pipes and ice lenses can increase the total equivalent surface σ^0 by $\sim$12 dB. So we define the day when the σ^0 value returns to within 3 dB of the 'mean winter backscatter' as the end-of-melt event. We specify January–March and November–December as the winter season and calculate the mean winter σ^0 during these months.

4. Results

[12] Figures 1b and 1c show melt extents and durations calculated from threshold based analysis of QuikSCAT σ^0 data and wavelet analysis of SSM/I Tb data for the 2001–2008 overlap period. Because QuikSCAT has a higher spatial resolution compared to SSM/I, the QuikSCAT melt duration maps vary more smoothly. The correlation coefficient of melt-extent time-series between the SSM/I estimates and the QuikSCAT estimates is 0.98 for the period 2000–2008. Unlike the EASE grid PM data, the high spatial resolution QuikSCAT data is an averaged σ^0 data measured over the period of a day. Hence there is a difference in observation time which results in a small difference in the melt-area observed by the two sensors. We also observe that QuikSCAT melt duration is slightly higher than PM estimates (Figure 1b). This is because our mean winter backscatter value is most likely conservative and hence we estimate a longer melt duration for QuikSCAT.

[13] We compare our results with PM derived melt estimates of *Joshi et al.* [2001] for 1979–1997 and with *Wang et al.*'s [2007] 2000–2004 QuikSCAT results (Figure 2a). Joshi et al. used a larger land mask and a different data projection for SSM/I and hence her estimates of annual surface melt-area are slightly biased compared to ours although the inter-annul variations are very similar. Our melt estimates from QuikSCAT for the period 2000–2004 overlap those of Wang (Figure 2a) and the correlation coefficient is 0.98.

5. Discussion

[14] Our surface melt-area time-series (Figure 2b) shows a persistent increase in melt-area after 1995. So rather than estimating a linear rate of increase for the entire record, we fit separate least square regression lines to the periods before and after 1995. We find that the surface melt-area

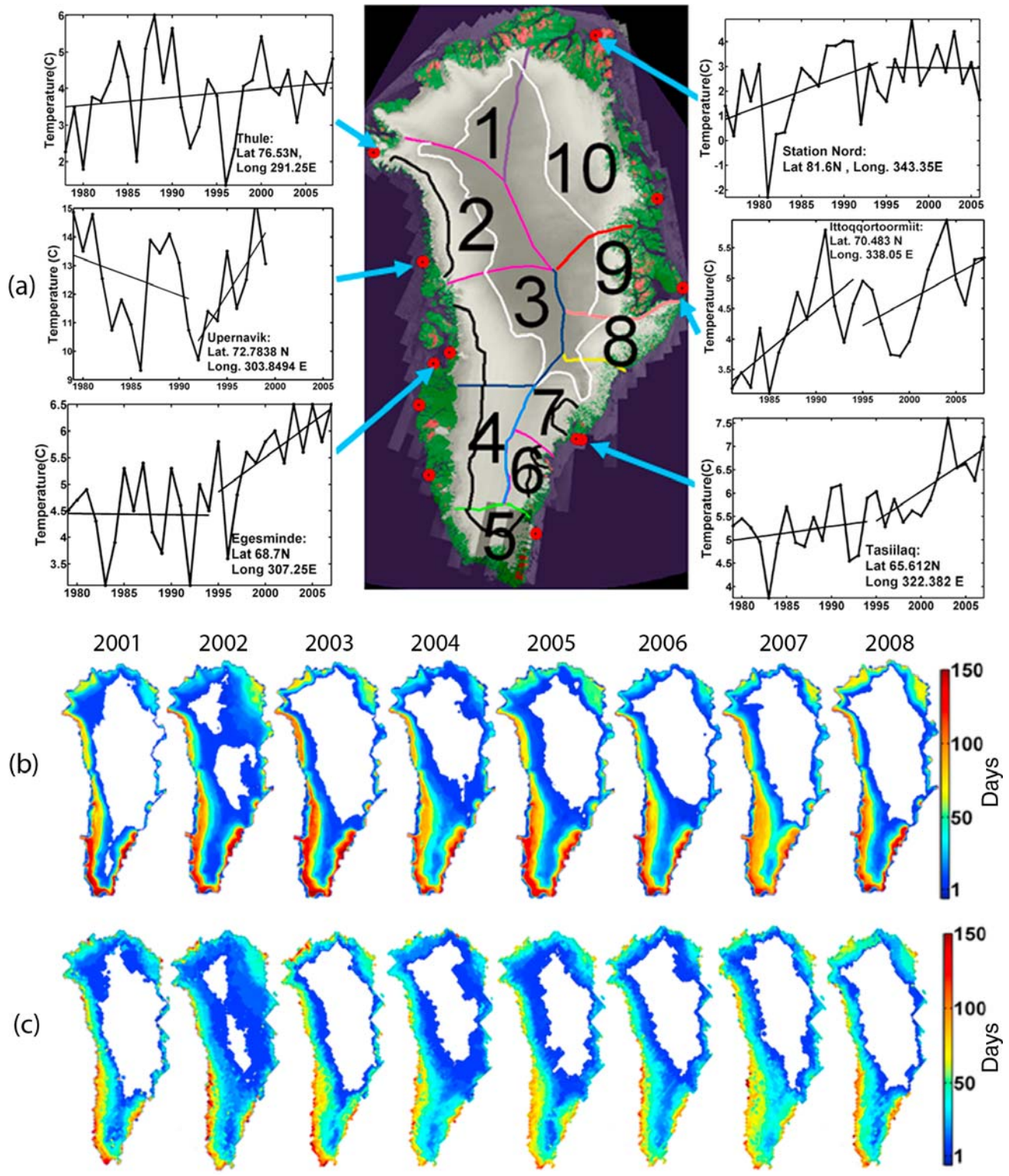

Figure 1. (a) Greenland Ice Sheet divided into 10 sectors and each sector further sub-divided into snow facies. The white line delineates the dry snow facies. The region between the black lines and the ice-sheet margin corresponds to wet facies, while regions in-between black and white lines correspond to percolation facies. The red dots corresponds to 12 coastal weather stations and associated annual temperature records. Melt extent and duration for GrIS for (b) 2001–2008 from QuikSCAT and (c) 2001–2008 from SSM/I.

increase at $7.64 \times 10^3 \pm 4.79 \times 10^3 km^2$/year between 1979–1994 where as the increase is only $9.64 \times 10^2 \pm 1.10 \times 10^4 km^2$/year between 1995–2008. The error for the melt-area trend from 1995–2008 is particularly large because of weighting by the anomalously high melt-area in 2002 and larger inter-annual variability after 1995. The 2002 melt event was probably caused by warm air advection steered by strong southerly flow associated with a high pressure

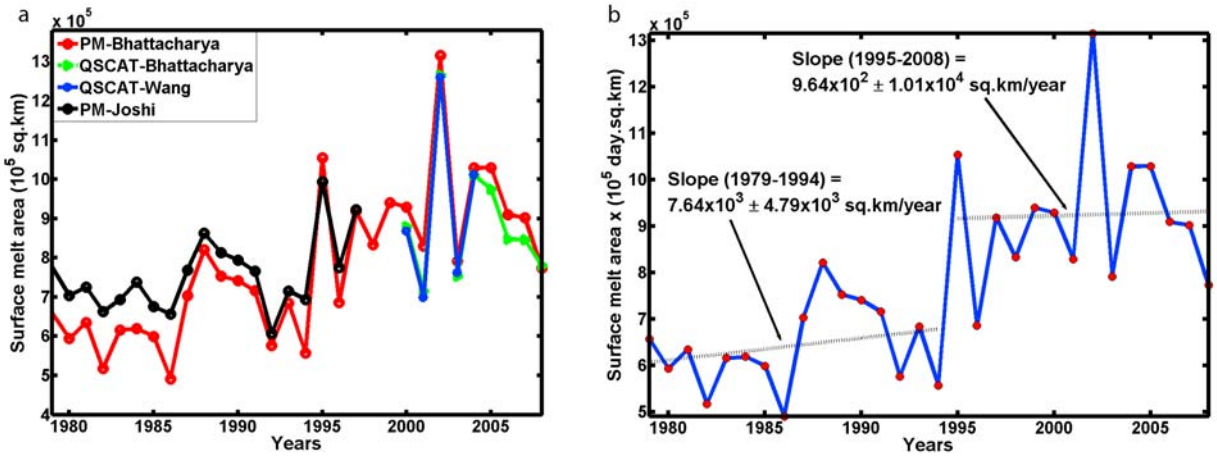

Figure 2. (a) Surface melt area comparison between QuikSCAT and PM from the present work and results of Joshi and Wang. (b) PM surface melt area and trends from 1979–2008 as calculated using the wavelet algorithm.

ridge extending over the GrIS from the North Atlantic Ocean [*Wang et al.*, 2007].

[15] The sector-wise melt-area percentage time-series of the GrIS show large inter-sector variability (Figures 3a, 3b, and 3c). Three out of four southerly sectors (4, 5, 6 in Figure 1a) have been melting completely since early 1990's and have little influence on the ice-sheet wide surface melt-area trend. Sector 7 shows a large inter-annual variability and also experiences maximum melt for nine years since the early 1990's. Sector 1 and 10 which constitutes the northerly part of the ice sheet, show large inter-annular variability and a general increase of $4.74 \times 10^3 \pm 1.37 \times 10^3 \mathrm{km}^2$/year in melt-area from 1979–2008. For sector 2, 3, 8 and 9 which constitutes the mid-section of the ice-sheet, the melt-area increases by $3.14 \times 10^3 \pm 2.54 \times 10^3 \mathrm{km}^2$/year till 1994 and from 1995–2008 the trend is statistically not different from zero. The melt area records for the central sectors of the ice sheet indicate a step-like increase starting in 1995

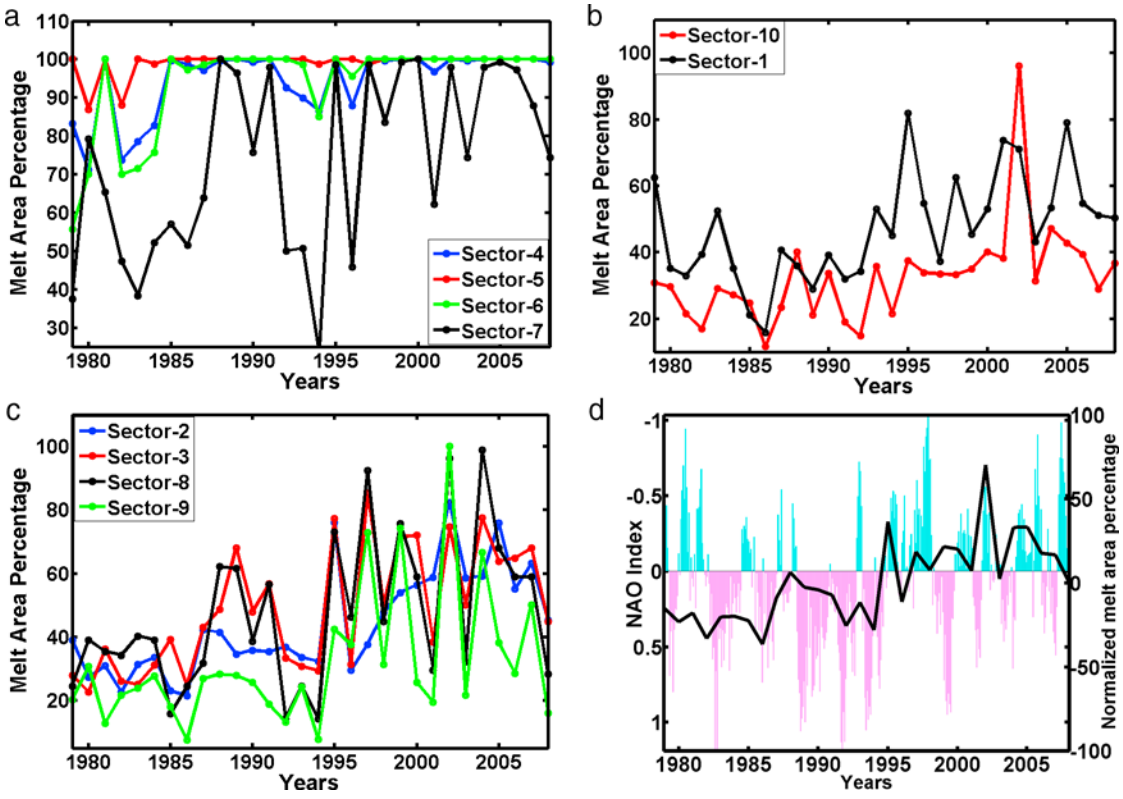

Figure 3. (a) The percentage change in melt-area time-series for three southerly sectors showing saturation in melt-area since 1990's and a fourth sector with large variability. (b) The percentage change in melt-area time-series for two northerly sectors with large variability and a linear increasing trend. (c) The percentage change in melt-area time-series for the four sectors with a prominent step-like increase in 1995. (d) Monthly NAO Index (smoothed by 6 months running average) and normalized annual melt-area percentage from 1979–2008.

but any such record is obscured in the south by melt area saturation. The record is more gradually varying for the northernmost sectors.

[16] To investigate correlation between the melt record and other climate data, we analyzed the mean summer temperature for 12 coastal weather stations (Figure 1a). We find two periods in the temperature records for 8 of the sites, similar to the observed trends in the sector-wise surface melt-area time-series. The mean summer temperature plots of 6 representative weather stations are shown in Figure 1a. In the northwest the temperature trend is slightly increasing at Thule which is situated near the boundary of sector 1 and 2. The available shorter time-series (1979–1999) of mean summer temperature at Upernavik (located in sector 2) reveals a warmer period between 1986 to 1992 that correlates well with elevated melt extent for sectors 2, 3, 8 and 9 (Figure 3c) although the strong early 1980's warming period at Upernavik seems only weakly reflected in the same melt records.

[17] At Station-Nord (sector 10), temperature increases till 1995 after which there is no discernable trend. The melt-area percentage time-series for sector 10 also shows similar behavior however the strong melt event in 2002 is not particularly observable as a warming in the coastal air temperature. The mean summer air temperature at Ittoqqortoormiit (in sector 9) is partitionable into two trends before and after 1995 but the temperature record does not clearly show the step-like change so evident in the surface melt record (Figure 3c). More to the south, temperature records at Tasiilaq (in sector 7) and Godthåb (in sector 4, temperature plot not shown) show a clear break at about 1995. However the melt records for the associated sectors are near saturation so any correlation with air temperature is masked. The temperatures at Ilulissat (in sector 3, temperature plot not shown) and Edgesminde (in sector 3) show a break in 1995 (Figure 1a) which correlates with the step-like increase in melt-area since 1995 (Figure 3b).

[18] Based on *Mote*'s [1998] observation of a relationship between Greenland surface melt and mid-tropospheric circulation, we investigated regional factors affecting the spatial variability of sector-wise melt-trend change in 1995. In particular we looked at NAO and its influence on the GrIS. NAO describes the variation of Arctic and sub-tropical Atlantic atmospheric masses and is quantified by the difference of surface pressure anomalies between Iceland and the Azores [*Thompson et al.*, 2005]. NAO variability has been linked with storm tracks, cyclones, sea-ice extent, precipitation patterns and temperature trends on the GrIS [*Calder et al.*, 2008].

[19] Studies of NAO and coastal air temperature of Greenland show that air temperature is inversely correlated with NAO index [*Box*, 2002; *Hanna and Cappelen*, 2003]. *Hanna et al.* [2008] later reported that the negative correlation of annual NAO and air temperature over GrIS has become weaker since the mid-1990's when the NAO index became more negative. *Holland et al.* [2008] reported a substantial increase in the subsurface ocean temperatures around the western coast of Greenland in 1997 and they related the warming with a sign-reversal of the NAO index during winter of 1995–1996. Figure 3d shows the comparison of normalized annual melt-area percentage (difference between annual melt-area and average melt-area for 30 years, divided by the average) and the monthly NAO index (smoothed by 6 months running average) from 1979–2008 (http://www.cpc.noaa.gov/products/precip/CWlink/pna/nao.shtml). We observe that the NAO index switches from predominantly positive to predominantly negative values in 1995. This event coincides with the step-like increase of melt area in 1995 and is consistent with the inverse relationship between air temperature and NAO index.

[20] The NAO does not affect the entire GrIS in a uniform manner. Results from *Thompson et al.* [2005] and *Calder et al.* [2008] show that the NAO modulation of snow accumulation over GrIS is most persistent along the northwest and west-central side and to a lesser extent in the southeast. Indeed, sectors 2 and 3, which show the step-like increase of melt-area since 1995 (Figure 3c), comprise most of the north-western and west-central area of the GrIS (Figure 1a). The mean summer temperature at coastal sites in these two sectors also shows an increase since 1995. But we also find a correlation between the step-like air temperature trend and the melt-area trend for sectors 8 and 9 which comprise the east-central part of the GrIS. This suggests a possible influence of NAO on the east-central temperature of the ice sheet too. We interpret the absence of a step change in melt-area for northerly sectors as evidence that the influence of changing NAO signal is not yet being felt at those latitudes. The influence of NAO on melt areas of our southerly sectors is masked by saturated melt signatures.

6. Conclusion

[21] We find a large spatial variability in the melt-area record of the GrIS. The melt-area time series of the ice-sheet is separable into a period before 1995 and a period after 1995. Before 1995 the melt area increase rate is greater than the rate after 1995 although there is larger inter-annual variability since 1995. The lower rate since 1995 can be partly explained by the fact that the southerly melt area record is essentially saturated and no longer contributes to the trends. The northerly melt area records are gradually increasing at a rate of $4.74 \times 10^3 \pm 1.37 \times 10^3 \mathrm{km}^2$/year (almost 1.05% per year of the total area of sector 1 and 10). At this rate the melt record in the north will become saturated in approximately 116 years. The mid-section of the ice-sheet, which constitutes approximately 22% of the entire GrIS, shows a brief increase in melt from 1985–1992 followed by a steep and persistent increase in melt-area starting in 1995. This 1995 event coincides with changes in summer temperature and a change of NAO index from positive to negative in the mid-1990's. Our melt analysis further suggests that a changing NAO affects both the central western and central eastern sides of the ice-sheet but not yet the northerly sectors.

[22] **Acknowledgments.** This work was funded by NASA's polar oceans and ice-sheet program and NSF's CRESIS project. We thank NSIDC in Boulder, Colorado, for providing the brightness temperature data. QuikSCAT data were provided by Brigham Young University Scatterometer Climate Record Pathfinder project. We thank David Long for his help. Finally we thank the editor and the anonymous reviewers for their constructive suggestions. This is Byrd Polar Research Center contribution 1388.

References

Abdalati, W., and K. Steffen (1997), Snowmelt on the Greenland ice sheet as derived from passive microwave satellite data, *J. Clim.*, *10*, 165–175, doi:10.1175/1520-0442(1997)010<0165:SOTGIS>2.0.CO;2.

Ashcraft, I. S., and D. G. Long (2006), Comparison of methods for melt detection over Greenland using active and passive microwave measurements, *Int. J. Remote Sens.*, *27*, 2469–2488, doi:10.1080/01431160500534465.

Box, J. E. (2002), Survey of Greenland instrumental temperature records: 1873–2001, *Int. J. Climatol.*, *22*, 1829–1847, doi:10.1002/joc.852.

Calder, C. A., P. F. Craigmile, and E. M. Thompson (2008), Spatial variation in the influence of the North Atlantic Oscillation on precipitation across Greenland, *J. Geophys. Res.*, *113*, D06112, doi:10.1029/2007JD009227.

England, A. W. (1976), Relative influence upon microwave emissivity of fine scale stratigraphy, internal scattering and dielectric properties, *Pure Appl. Geophys.*, *114*, 287–299, doi:10.1007/BF00878953.

Hanna, E., and J. Cappelen (2003), Recent cooling in coastal southern Greenland and relation with the North Atlantic Oscillation, *Geophys. Res. Lett.*, *30*(3), 1132, doi:10.1029/2002GL015797.

Hanna, E., P. Huybrechts, K. Steffen, J. Cappelen, R. Huff, C. Shuman, T. Irvine-Fynn, S. Wise, and M. Griffiths (2008), Increased runoff from melt from the Greenland ice sheet: A response to global warming, *J. Clim.*, *21*, 331–341, doi:10.1175/2007JCLI1964.1.

Holland, M. D., R. H. Thomas, B. D. Young, and M. H. Ribergaard (2008), Acceleration of Jakobshavn Isbræ triggered by warm subsurface ocean waters, *Nat. Geosci.*, *1*, 659–664, doi:10.1038/ngeo316.

Jezek, K. C., C. J. Merry, and D. J. Cavalieri (1993), Comparison of SMMR and SSM/I passive microwave data collected over Antarctica, *Ann. Glaciol.*, *17*, 131–136.

Joshi, M., C. J. Merry, K. C. Jezek, and J. F. Bolzan (2001), An edge detection technique to estimate melt duration season and melt extent on the Greenland ice sheet using passive microwave data, *Geophys. Res. Lett.*, *28*, 3497–3500, doi:10.1029/2000GL012503.

Liu, H., L. Wang, and K. C. Jezek (2005), Wavelet transform based edge detection approach to derivation of snowmelt onset, end and duration from satellite passive microwave measurements, *Int. J. Remote Sens.*, *26*, 4639–4660, doi:10.1080/01431160500213342.

Liu, H., L. Wang, and K. C. Jezek (2006), Spatiotemporal variations of snowmelt in Antarctica derived from satellite scanning multichannel microwave radiometer and special sensor microwave imager data (1978–2004), *J. Geophys. Res.*, *111*, F01003, doi:10.1029/2005JF000318.

Mote, T. L. (1998), Mid-Tropospheric circulation and surface melt on the Greenland ice sheet. Part II: Synoptic climatology, *Int. J. Climatol.*, *18*, 131–145, doi:10.1002/(SICI)1097-0088(199802)18:2<131::AID-JOC228>3.0.CO;2-S.

Mote, T. L. (2007), Greenland surface melt trends 1973–2007: Evidence of a large increase in 2007, *Geophys. Res. Lett.*, *34*, L22507, doi:10.1029/2007GL031976.

Nghiem, S. V., K. Steffen, R. Kwak, and W. Y. Tsai (2001), Detection of snowmelt regions on Greenland ice sheet using diurnal backscatter change, *J. Glaciol.*, *47*, 539–547, doi:10.3189/172756501781831738.

Steffen, K., S. V. Ngheim, R. Huff, and G. Neumann (2004), The melt anomaly of 2002 on the Greenland ice sheet from active and passive microwave satellite observations, *Geophys. Res. Lett.*, *31*, L20402, doi:10.1029/2004GL020444.

Stroeve, J., M. Serreze, S. Drobot, S. Gearheard, M. Holland, J. Maslanik, W. Meier, and T. Scambos (2008), Arctic sea ice extent plummets in 2007, *Eos Trans. AGU*, *89*(2), doi:10.1029/2008EO020001.

Tedesco, M. (2007), Snowmelt detection over the Greenland ice sheet from SSM/I brightness temperature daily variations, *Geophys. Res. Lett.*, *34*, L02504, doi:10.1029/2006GL028466.

Thompson, E. M., C. R. Readinger, P. Craigmile, L. G. Thompson, and C. A. Calder (2005), Regional sensitivity of Greenland precipitation to NAO variability, *Geophys. Res. Lett.*, *32*, L24707, doi:10.1029/2005GL024776.

Wang, L., M. Sharp, B. Rivard, and K. Steffen (2007), Melt season duration and ice layer formation on the Greenland ice-sheet, 2000–2004, *J. Geophys. Res.*, *112*, F04013, doi:10.1029/2007JF000760.

Zabel, I. H. H., K. C. Jezek, P. A. Baggeroer, and S. P. Gogineni (1995), Ground-based radar observations of snow stratigraphy and melt processes in the percolation facies of the Greenland ice sheet, *Ann. Glaciol.*, *21*, 40–44.

I. Bhattacharya and K. C. Jezek, Byrd Polar Research Center, Ohio State University, 1090 Carmack Rd., Columbus, OH 43210, USA. (bhattacharya.21@gmail.com)

H. Liu, Department of Geography, University of Cincinnati, 401 Braunstein Hall, Cincinnati, OH 45221, USA.

L. Wang, Department of Geography and Anthropology, Louisiana State University, 227 Howe-Russell Geoscience Complex, Baton Rouge, LA 70803, USA.